Scale Evolution of Finite-Amplitude Instabilities on a Coastal Upwelling Front

SCOTT M. DURSKI, J. S. ALLEN, G. D. EGBERT, AND R. M. SAMELSON

College of Oceanic and Atmospheric Sciences, Oregon State University, Corvallis, Oregon

(Manuscript received 19 October 2005, in final form 14 June 2006)

ABSTRACT

Nonlinear model simulations of a coastal upwelling system show frontal instabilities that initiate at short alongshore scales but rapidly evolve to longer wavelengths. Several factors associated with the nonstationarity of this basic state contribute to the progression in scale. A portion of the system evolution is associated with the external forcing. Another portion is associated with the alteration of the alongshore mean flow resulting from wave growth. Direct interactions between the finite-amplitude disturbances also promote emergence of new scales. The relative role of each of these mechanisms is isolated through tangent linear simulations about basic states that approximate the nonlinear system to differing degrees. The basic states include an alongshore uniform time-evolving upwelling solution, the alongshore average of a three-dimensionally evolving upwelling solution, and the full three-dimensional nonlinear solution. Disturbance growth about a frozen-field upwelling state is also examined. Perturbation experiments are performed for persistent and relaxed wind forcing. Although the frontal disturbances in the nonlinear model exhibit a progression to larger scale over the full range of forcing scenarios considered, the mechanisms most responsible for the process differ between wind-forced and unforced cases. Under relaxed wind conditions, the perturbation growth experiments indicate that the scale evolution over the first four days is reflected in the way linear disturbances respond to the adjustment of an alongshore uniform upwelling front to wind cessation. The continued increase in scale between days 4 and 7 is related to the linear disturbance evolution on the alongshore average of a flow state that has been altered by wave–mean flow interaction. Past day 7, the observed scale change is not captured in the linear growth experiments and evidently results largely from nonlinear wave–wave interaction processes. Under sustained upwelling winds, the linear growth experiments fail to describe even the earliest scale change in the nonlinear solutions, indicating that nonlinear wave–wave effects are significant from very near the start of the simulations.

1. Introduction

Coastal upwelling fronts often exhibit meanders and deflections on many different scales. As these disturbances become large they can produce eddies, squirts, and filaments that transport significant amounts of biologically and chemically important substances off the shelf. The factors that influence the observed scales are many, including bathymetric variations, coastline curvature, and inhomogeneity in the wind field. But complex frontal structures are not uncommon even in numerical simulations of upwelling fronts with uniform winds, alongshore uniform bathymetry, and straight coastlines. In these cases it is the hydrodynamic instability of the flow that introduces the initial scales of variability. Normal mode analyses based on stationary representations of the background upwelling flow structure yield approximations to the disturbances that exhibit the fastest asymptotic growth (Barth 1989a,b, 1994; McCreary et al. 1991; Fukamachi et al. 1995; Shi and Roed 1999; Eldevik and Dysthe 2002). Typically, though, the upwelling wind forcing dictates a continuously changing displacement of the front, so the relevance of a linear analysis about any particular snapshot or averaged representation of the flow state might be questioned. The relationship between the leading normal modes and the observed disturbances becomes more ambiguous still as the disturbance amplitude becomes large enough to significantly alter the underlying circulation.

Durski and Allen (2005) examined the finite-amplitude evolution of instabilities associated with a coastal upwelling front using a primitive equation ocean

Corresponding author address: Dr. Scott M. Durski, College of Oceanic and Atmospheric Sciences, Oregon State University, 104 COAS Admin. Bldg., Corvallis, OR 97331.
E-mail: sdurski@coas.oregonstate.edu

DOI: 10.1175/JPO2994.1

model. They noted that in a periodic channel domain with alongshore uniform bathymetry and stratification typical of summer conditions off the Oregon coast frontal meanders emerged in response to sustained wind forcing at an 8–10-km scale, but that within 10 days the predominant scale grew by a factor of 4 to 5. During this process, waves appeared to increase in amplitude and merge into larger alongshore scale structures. The analysis suggested that the scale change resulted from the interaction of waves that developed at small scale, rather than from the accelerated growth of longer-wavelength instabilities as the background flow evolved. However, a comprehensive investigation of the dynamical processes responsible for the scale change was not pursued.

In the present study, the relative contribution of different mechanisms to the observed alongshore scale transformation is diagnosed by comparison of linear perturbation growth on a range of time-varying basic-state flows that represent varying degrees of approximation to the full nonlinear model evolution. By specifying basic state flows as 1) the unperturbed alongshore uniform upwelling evolution, 2) the alongshore average of the perturbed upwelling flow, and 3) the full three-dimensional perturbed upwelling evolution, the effect on scale change due to the wind forcing, wave–mean flow interaction, and wave–wave effects is elucidated. Background states with sustained and relaxed wind forcing are examined to explore how winds alter the disturbance growth characteristics.

2. Model setup

a. Approach

This study involves numerical simulations with the hydrostatic, primitive equation Regional Ocean Model System (ROMS) (Shchepetkin and McWilliams 2003) (denoted NLM below) and the tangent linear to that model (denoted TLM below) (Moore et al. 2004). Expressed symbolically, if the NLM is

$$\frac{\partial \mathbf{S}}{\partial t} = \mathbf{N}(\mathbf{S}), \tag{1}$$

where $\mathbf{S}$ is the model state vector and $\mathbf{N}$ is the nonlinear model operator, then a first-order Taylor expansion of $\mathbf{N}$ about a solution state S_o yields the TLM,

$$\frac{\partial \mathbf{s}}{\partial t} = \frac{\partial \mathbf{N}(\mathbf{S})}{\partial \mathbf{S}}\bigg|_{S_o} \mathbf{s} = \mathbf{A}\mathbf{s}, \tag{2}$$

where $\mathbf{s}$ represents a perturbation and $\mathbf{A}$ is a linear operator. The TLM provides a means to examine linear disturbance growth about a nonlinear model solution and also affords the possibility of studying perturbation trajectories about meaningful idealizations of those solutions.

The goal of this study is to develop an understanding of the mechanisms responsible for scale change on a coastal upwelling front by examination of disturbance evolution in a series of approximations to the nonlinear solutions. Linear disturbances on a stationary alongshore uniform upwelling front converge to the scale and modal structure that amplifies most rapidly on that fixed background state. Temporal evolution of S_o introduces the possibility that different perturbation scales and structures will be favored at different times. A nonlinear simulation of an unperturbed upwelling front presents a temporally changing (but always alongshore uniform) flow structure. A TLM simulation about this time-dependent nonlinear basic state exposes the degree to which the upwelling process itself promotes evolution to larger scales. Nonlinear model integrations with a perturbation added to the alongshore uniform upwelling state develop instabilities at small scale that amplify and advance to larger scale. The finite-amplitude evolution of the disturbances may alter the alongshore mean state so that it favors growth at lower wavenumbers. TLM simulations about the alongshore average of the perturbed background state thus indirectly include the effect of wave–mean flow feedback (where the waves providing the feedback are those that develop in the nonlinear base experiment). It is also possible that larger scales may become favored for growth about the developing wavy background state but not about its alongshore average. For example wave–wave interactions among the finite-amplitude instabilities may preferentially promote larger scales. Although a TLM simulation cannot describe this nonlinear process explicitly, the spatial relationship between the growing linear disturbances and the full perturbed nonlinear model solution provide useful insight into how these instabilities modify the total flow. The nonlinear analog to these TLM simulations, which is also examined here, is the difference between nonlinear simulations perturbed slightly differently at the onset of their integrations.

b. NLM simulations—The basic states S_o

The NLM configuration is identical to that used in Durski and Allen (2005) except that horizontal viscosity and diffusivity are set to zero and the offshore boundary is a solid wall. The domain is a 240-km-long, 75-km-wide periodic channel. A Cartesian coordinate is used with x aligned along-channel and y aligned across channel. The bathymetry is specified as an alongshore uniform, smoothed representation of the typical across-

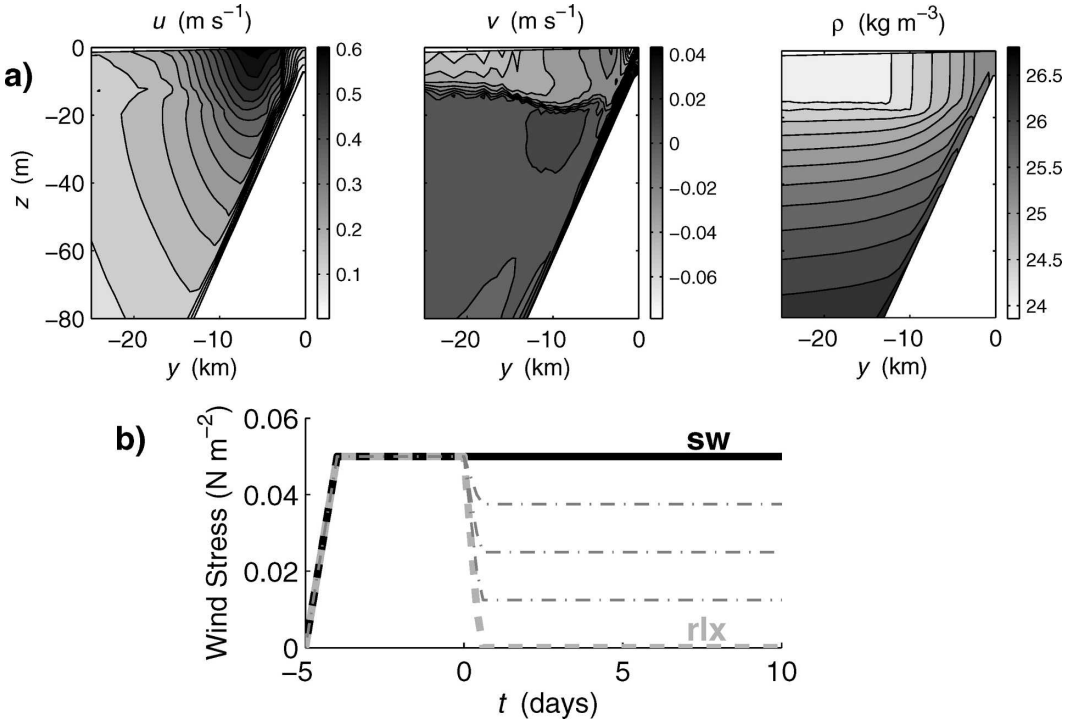

FIG. 1. (a) Alongshore velocity u, across-shore velocity v, and potential density ρ across-shelf (y, z) sections of the initial unperturbed background state. (b) Schematic of the forcing for the relaxed wind (rlx) and steady wind (sw) experiments. In both cases the model is "spun up" with 5 days of upwelling favorable winds prior to the start of the disturbance growth experiments. The intermediate level lines reference the wind forcing in the partially sustained wind experiments.

shore depth profile off the coast of Oregon. The bottom drops from 6-m depth at the coast (at $y = 0$ km) to 1000-m depth at the offshore wall ($y = -75$ km). The horizontal grid resolution is 1 km in the alongshore direction. In the cross-shore direction stretched grid spacing gives approximately uniform 500-m resolution inshore of $y = -35$ km expanding to 5-km resolution at the offshore boundary ($y = -75$ km). Thirty vertical sigma levels are employed. In this study, potential density ρ is used in place of temperature and salinity.

The initial state for the disturbance growth experiments (Fig. 1a) is the unperturbed (alongshore uniform) nonlinear model state after a 5-day spinup of upwelling favorable winds. The nonlinear model is started from a state of rest at $t = -5$ days, with an initial density profile based on summer field observations off the Oregon Coast. A 0.05 N m^{-2} upwelling favorable wind stress is ramped up over half a day and is sustained for an additional 4.5 days to attain an initial alongshore uniform, developed upwelling state on which disturbance growth studies are initiated (Fig. 1b). By this time an upwelling front with an associated alongshore jet with maximum speeds of 60 cm s^{-1} has been established. Two model evolutions are considered from this point to examine the effect of relaxation or continuation of the winds (Fig. 1b). In the relaxed wind experiments (RLX) the wind stress is decreased to zero between days 0 and 0.5. In the steady (persistent) wind experiments (SW), the wind stress is maintained at 0.05 N m^{-2}. Partial wind relaxation is considered in section 3b(2): in those experiments, the wind forcing decreases after day 0 to new sustained levels of 0.0375, 0.025, and 0.0125 N m^{-2}.

Basic states for the disturbance growth experiments are generated by integration of the NLM with or without an initial small perturbation in the alongshore direction. Perturbations are defined as deviations from the alongshore average such that

$$u = \langle u \rangle + u' \quad \text{and} \tag{3}$$

$$\langle u' \rangle = 0, \tag{4}$$

where the angle brackets denote the alongshore average of a field,

$$\langle u \rangle = \frac{1}{L_x} \int_0^{L_x} u \, dx, \tag{5}$$

with L_x the length of the domain in x.

The four basic states are

- S_o^F—a stationary and unperturbed NLM solution:

$$S_o^F(y, z) = \int_{t_b}^{t_s} N(S)\, dt' + S(t = t_b), \tag{6}$$

where t_b is day -5 and t_s is day 0, and $S(t = t_b)$ is alongshore uniform,

- S_o^{2D}—an unperturbed alongshore uniform time-evolving NLM solution:

$$S_o^{2D}(y, z, t) = S_o^F + \int_{t_s}^{t} N(S)\, dt', \tag{7}$$

with $S(t = t_s) = S_o^F$,

- S_o^{3D}—a three-dimensionally evolving, perturbed NLM solution:

$$S_o^{3D}(x, y, z, t) = S_o^F + S' + \int_{t_s}^{t} N(S)\, dt', \tag{8}$$

where $S(t = t_s) = S_o^F(y, z) + S'(x, y, z)$ and S' represents a perturbation from the alongshore average, and

- $S_o^{\langle 3D\rangle}$—the alongshore average of a perturbed NLM solution:

$$S_o^{\langle 3D\rangle}(y, z, t) = \langle S_o^{3D}\rangle. \tag{9}$$

Similar notation will be used to distinguish different model runs. For example, $\mathrm{TL}^{\langle 3D\rangle}$ refers to a tangent linear model experiment about the alongshore average of a perturbed nonlinear model solution. Nonlinear disturbance growth experiments in which the nonlinear model is integrated forward with an additional small initial perturbation

$$S(t = t_s) = S_o^F + S' + S'', \tag{10}$$

where S'' is two orders of magnitude smaller than S', will be denoted NL^p.

c. The tangent linear model

Computationally, the TLM was implemented by Moore et al. (2004) directly from the FORTRAN code of ROMS using the recipes of Giering and Kaminski (1998). The domain configuration and model settings (linearized advection scheme, boundary conditions, etc.) are all identical to those in the nonlinear setup. All basic states are obtained from the nonlinear model runs as described above. Time-evolving background states S_o, are approximated by linear interpolation between snapshots from the NLM. For this study, the basic-state fields are interpolated between snapshots that are 60 min (15 internal time steps) apart. Sensitivity tests revealed this to be the optimal interval for retaining solution quality while minimizing storage requirements. Note that the vertical viscosity and diffusivity coefficients determined from the nonlinear background flow [using Mellor and Yamada (1982) level 2.5] are used in the TLM. The terms arising from the linearization of the flow-dependent mixing coefficients are set equal to zero.

d. Initial perturbations, diagnostics, and the TL^F solution

An initial disturbance is required to initiate the instability processes in the basic-state nonlinear runs and to set off disturbance growth in the tangent linear and nonlinear perturbation experiments. In each case this perturbation is applied in u (alongshore velocity), v (across-shore velocity), and ρ (density). Care is taken in choosing this initial structure to minimize the transient adjustments at startup. The perturbation structures that are chosen are those that emerge from a random initial disturbance at each along-channel wavenumber k, after a 40-day integration of the tangent linear model on the day-0 alongshore uniform upwelling state S_o^F (Fig. 1a). High wavenumber signals are eliminated and perturbations are constructed from the spectral components between 6 and 240-km alongshore wavelengths. The amplitudes of the signals are normalized so that the total volume integrated energy

$$E_p(k) = \int\int e_p(y, z, k)\, dy\, dz \tag{11}$$

at each wavenumber is uniform. Here, the energy density $e_p(k)$ associated with disturbances at a given wavenumber k is approximated as

$$e_p(y, z, k) = \frac{1}{2}\rho_o\left[u_p^2(y, z, k) + v_p^2(y, z, k)\right] + \frac{g}{2}\left[\frac{\partial \rho_b(y, z)}{\partial z}\right]^{-1}\rho_p^2(y, z, k), \tag{12}$$

where ρ_o is 1000 kg m^{-3}, u_p and v_p are the perturbation horizontal velocity components, ρ_b is the background potential density anomaly, ρ_p is the perturbation potential density anomaly, and g is the gravitational acceleration. Although the quadratic term in density is only an exact representation of available potential energy in the limit of small-amplitude perturbations from a resting state (Shepherd 1993), it is deemed adequate for the diagnostic purposes considered here.

A set of disturbances are generated with different relative random phase shifts of the spectral components for use in generating ensembles of $\mathrm{TL}^{\langle 3D\rangle}$, TL^{3D}, and NL^p simulations. Each TL ensemble member describes a unique perturbation about the same nonlinear back-

ground state. The NL^p experiments each have an additional small initial perturbation applied about the same base nonlinear model initial state.

A useful diagnostic for quantifying the alongshore scale change is the energy-weighted mean alongshore wavenumber k_{mean},

$$k_{\text{mean}} = \frac{\int kE_p(k)\,dk}{\int E_p(k)\,dk}, \tag{13}$$

where the integral is over all resolved wavenumbers $k > 0$. The initial uniform distribution of energy in the perturbations gives at day 0, $\lambda_{\text{mean}} = 2\pi/k_{\text{mean}} \approx 13.5$ km^{-1}, for all simulations. Alternatively, a potential enstrophy weighted mean wavenumber k^Z_{mean} can be defined,

$$k^Z_{\text{mean}} = \frac{\int kZ(k)\,dk}{\int Z(k)\,dk}, \tag{14}$$

based on the potential enstrophy

$$Z = \left[-\frac{\partial v}{\partial z}\frac{\partial \rho}{\partial x} + \frac{\partial u}{\partial z}\frac{\partial \rho}{\partial y} + \left(\frac{\partial v}{\partial x} - \frac{\partial u}{\partial y} + f\right)\frac{\partial \rho}{\partial z}\right]^2 \tag{15}$$

(written here in Cartesian coordinates, but calculated in sigma coordinates for the analysis); f is the Coriolis parameter.

The long time integrations of TL^F (on the stationary background state S^F_o) from the random initial perturbations are used to attain an estimate of the growth rates of the initial perturbation structures as a function of wavenumber (Fig. 2). This is done by Fourier transforming the alongshore signal of density perturbation to separate out the amplitude response at different wavenumbers. A linear regression on the logarithm of the amplitude versus time yields an estimate of the growth rate of the fastest-growing mode at each scale. The fastest-growing scale of disturbance is a shallow, narrow frontal instability of approximately 11.4-km alongshore wavelength with a modal structure that appears symmetric about the upwelling jet maximum. A secondary peak in growth rate appears at approximately 40-km wavelength. The modal structure in this case is not symmetric about the jet and extends much farther offshore and deeper than the fastest-growing frontal instability. Disturbances with scales less than 8 km or greater than 60 km are damped (stable).

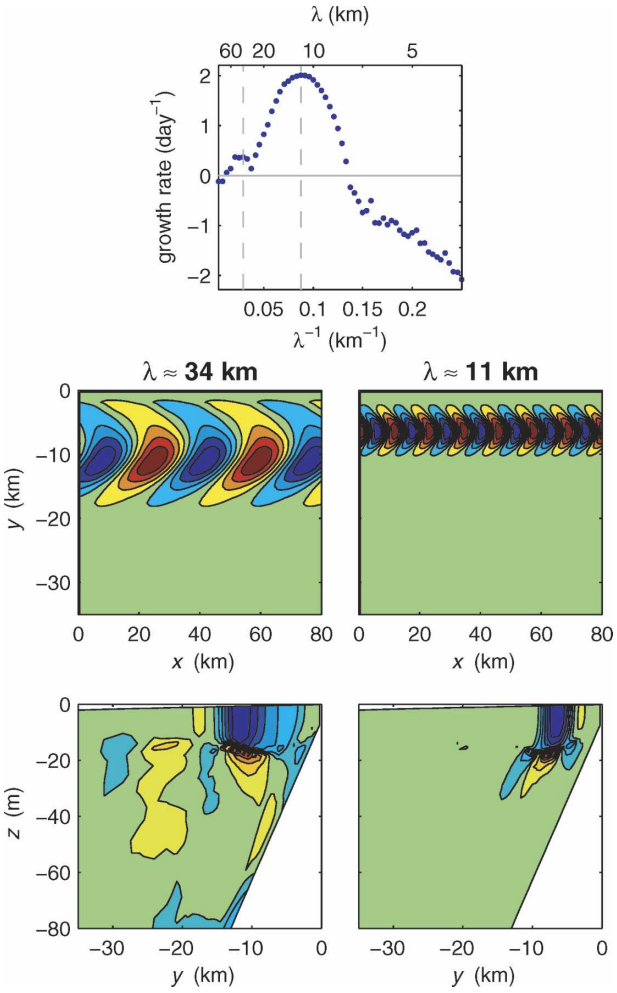

FIG. 2. (top) A growth-rate-curve estimate for the stationary initial state shown in Fig. 1a. (middle), (bottom) The modal structure of the density field for length scales of 40 and 11 km. (Red contours indicate high positive values and blue ones indicate large negative values, with the zero contour in the green range.) Depth sections display the fields at $x = 40$ km.

3. Results

a. Relaxed winds (case RLX)

1) NLM RESPONSE

In the NLM, the alongshore uniform (NL^{2D}) upwelling front responds to wind relaxation after $t = 0$ with moderate shoreward slumping of the isopycnals (Fig. 3). The depth structure of the alongshore jet changes only slightly, and the maximum surface jet velocity essentially maintains its magnitude and position. Much of the flow adjustment occurs within the first 3 days of the relaxation after which the circulation exhibits only a very gradual frictional decay.

When small perturbations with alongshore variability are added to the circulation at day 0 (NL^{3D}), frontal

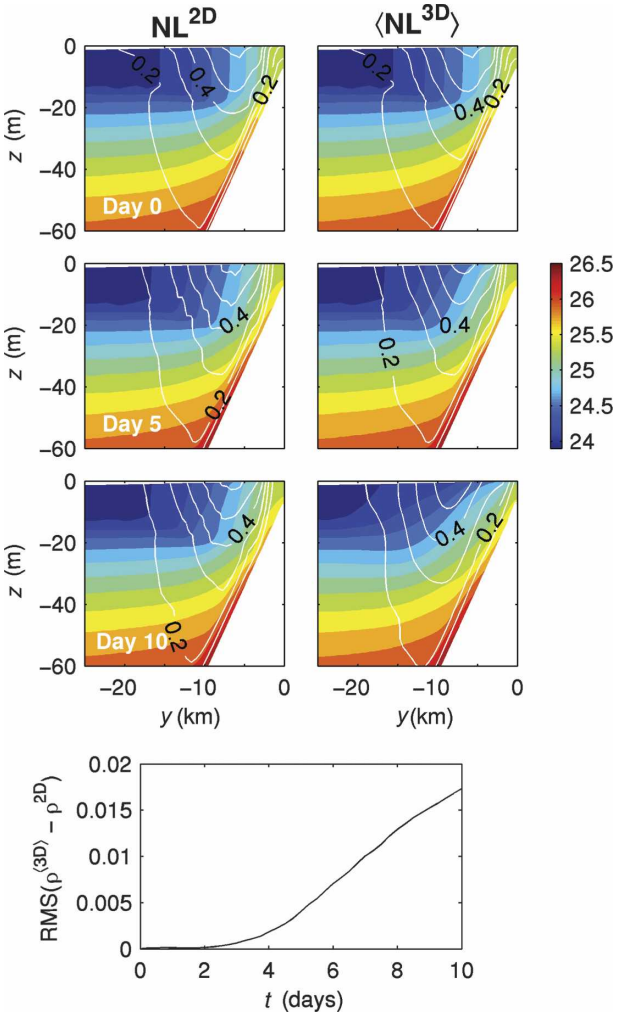

FIG. 3. (left, top three panels) Density (grayscale contours) and alongshore velocity (line contours) structure in an across-shore section for days 0, 5, and 10 for the unperturbed nonlinear wind relaxation experiment. (right, top three panels) The alongshore averages of the same fields for a perturbed nonlinear wind relaxation experiment. These fields are the background states (left) S_o^{2D} and (right) $S_o^{\langle 3D\rangle}$; (bottom) time series of the area (y–z) averaged rms difference in density between the two cases.

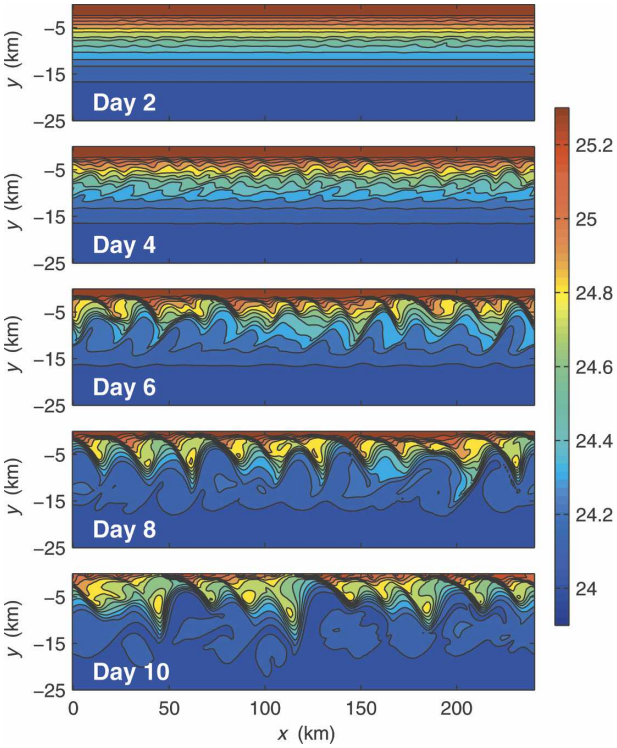

FIG. 4. Surface density contours depicting the evolution of the frontal instabilities in the nonlinear model wind relaxation experiments. Coastline is at $y = 0$.

instabilities develop rapidly (Fig. 4). By day 4, frontal meanders with sharp offshore crests are visible in the surface density field at approximately 14-km wavelength. Similar to the phenomenology noted under sustained winds in Durski and Allen (2005), these features grow in amplitude, interact, and appear to coalesce into larger-scale structures. Ten days into the simulation, features with scales as large as 80 km have developed on the front, and the intensity of shorter-wavelength structures has diminished. This process of alongshore scale evolution is the focus of this research. The analysis that follows focuses primarily on alongshore patterns because throughout the simulation the disturbances remain wavelike with an alongshore orientation (Fig. 4).

The scales that emerge first from the initially spectrally uniform disturbances in the NL^{3D} simulation average approximately 11.5 km (Fig. 5). But the mean along-channel wavelength λ_{mean} increases steadily to approximately 33 km by day 10. The normalized rate of change of $E_p(k)$ can be used to distinguish between scale increases due to enhanced growth at a given scale and enhanced decay at a shorter one (Fig. 6). The nonlinear model exhibits growth across a narrowing portion of the spectrum centered about the decreasing k_{mean} over the first 3 days. Between days 3 and 5, the rate of increase of energy at the predominant 15-km scale gradually diminishes and becomes negative. Simultaneously, there is a rapid increase in energy near a 20-km scale. This is suggestive of a wave–wave interaction, promoting longer-wavelength disturbances at the cost of the shorter-wavelength ones. A similar pattern appears between days 7 and 9 when the rate of energy increase at 20 km diminishes in concert with a strong energy increase at 80 km. After transient adjustment over the first 2 days, k^Z_{mean} displays a very similar evolution in scale (Fig. 5). This is in contrast to the situation in two-dimensional turbulence in which enstrophy cascades toward smaller scales.

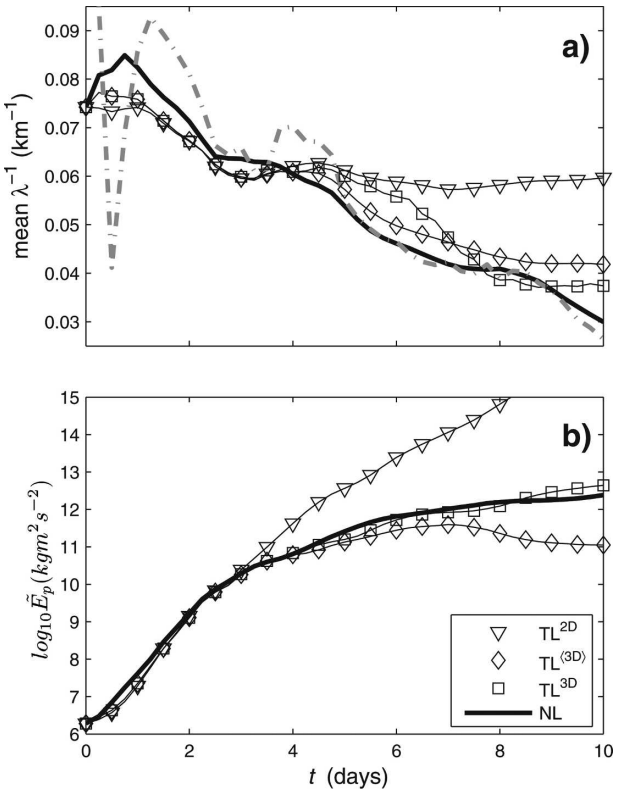

FIG. 5. (a) The mean alongshore wavenumber k_{mean} from Eq. (13) vs t for the relaxed wind nonlinear and tangent linear experiments along with k^Z_{mean} from Eq. (14) (gray dash–dot line) for the NL experiment. (b) Total perturbation energy $\tilde{E}_p$ vs t for the relaxed wind nonlinear and tangent linear experiments.

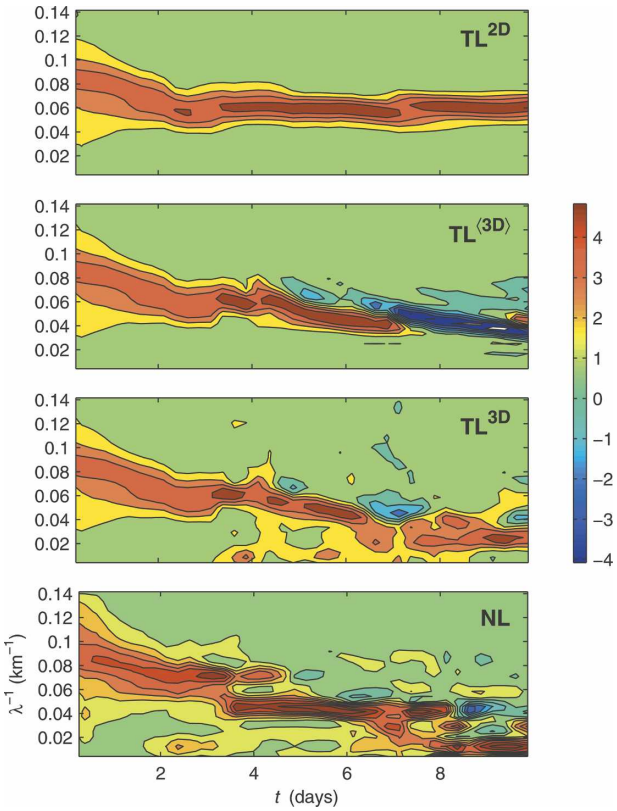

FIG. 6. The time rate of change of $E_p(k)$ as a function of wavenumber $\partial E_p(k)/\partial t$, normalized by the standard deviation of the rate of change at each time for the relaxed wind nonlinear and tangent linear experiments. The vertical axes are the inverse along-channel wavelength $\lambda^{-1} = k/2\pi$.

The rate at which total disturbance energy

$$\tilde{E}_p = \int E_p(k)\, dk \tag{16}$$

increases in the nonlinear model (Fig. 5) is roughly uniform over the first 3 days and then gradually tapers off. Over the last 2 days of the simulation, little additional energy is entering the disturbance scales from the mean flow, yet k_{mean} is still decreasing. This is again suggestive that in the later stages the scale change results from disturbance energy being redistributed to longer scales through wave–wave interactions.

2) TL^{2D} RESULTS

The TL^{2D} simulation describes linear growth of an initial disturbance about the S_o^{2D} background state (Figs. 3, 7). The evolution of cross-shore disturbance structure reflects the progression of one predominant scale being gradually replaced by a longer one. Roughly 12-km scale perturbations initially amplify preferentially at and offshore of the position of maximum alongshore velocity (Fig. 7), in contrast to the TL^F simulation in which the structure of the fastest-growing mode was symmetric about the jet axis (Fig. 2). The structure of the TL^{2D} growing disturbances changes as the simulation progresses. By day 10, the amplification of the disturbance within 2 km of the jet center dominates the surface pattern. It has a structure similar to that 8 days earlier but with a longer alongshore wavelength (16 km). The vertical structure in rms perturbation density in TL^{2D} resembles the nonlinear model results through approximately day 4 (Fig. 9, described below). Early in the experiment growth is concentrated at the surface and at approximately 20-m depth (Fig. 9, described below). As the simulation continues, TL^{2D} disturbances remain patchy and primarily focused at these two depths while the perturbation density distribution in the nonlinear model exhibits a broader, smoother structure with less intensification at depth.

The time series of mean alongshore wavenumber k_{mean} corroborates the progression in alongshore scale (Fig. 5). Over the first 3 days of the simulation k_{mean}

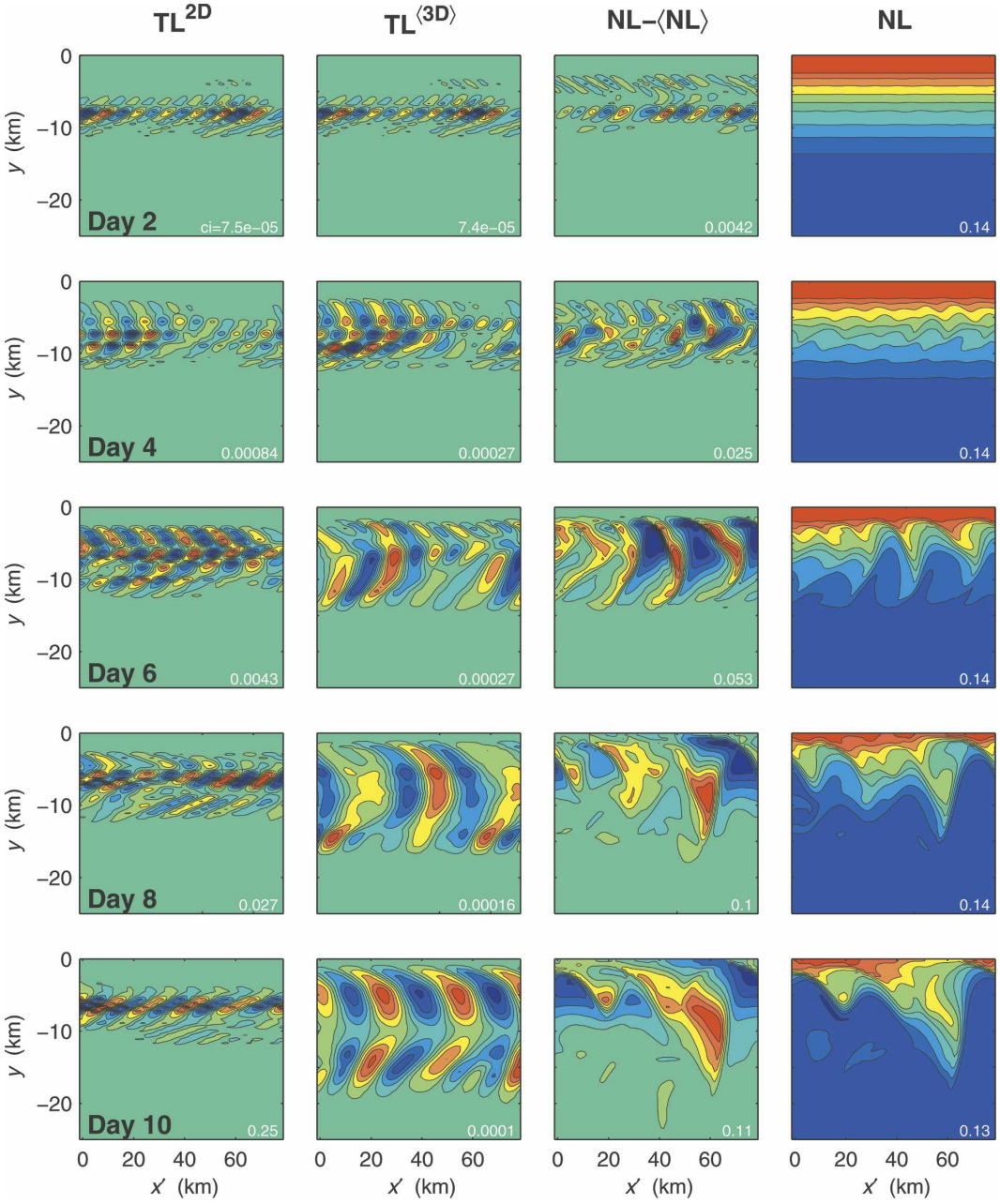

FIG. 7. Relaxed wind surface perturbation density signature of the disturbance evolution for (far left panels) the TL^{2D} simulation and (panels second from left) a single realization of $TL^{\langle 3D \rangle}$. Also plotted are (far right panels) surface density evolution for the corresponding perturbed nonlinear model and (panels second from right) the deviation from the alongshore average of the surface density in the nonlinear model. The 80-km region plotted tracks a propagating disturbance as it traverses the domain at a speed of approximately 0.28 m s^{-1}. Numbers in the lower-right corner of each panel indicate the contour interval for that frame. The zero contour in the three left-hand sets of panels is indicated by the color offshore.

declines in conjunction with the period during which the bulk of the adjustment of the flow structure to the wind relaxation occurs. Afterward, there is little further change in k_{mean}. Although there is no strong decay of disturbances at any wavenumber, the fastest-growing scale gradually increases from 12 to 16 km between days 0 and 3 (Fig. 6). For the remainder of the simulation, disturbance structure continues to evolve but growth remains largest at this scale.

For the first 3 days, many aspects of this solution are

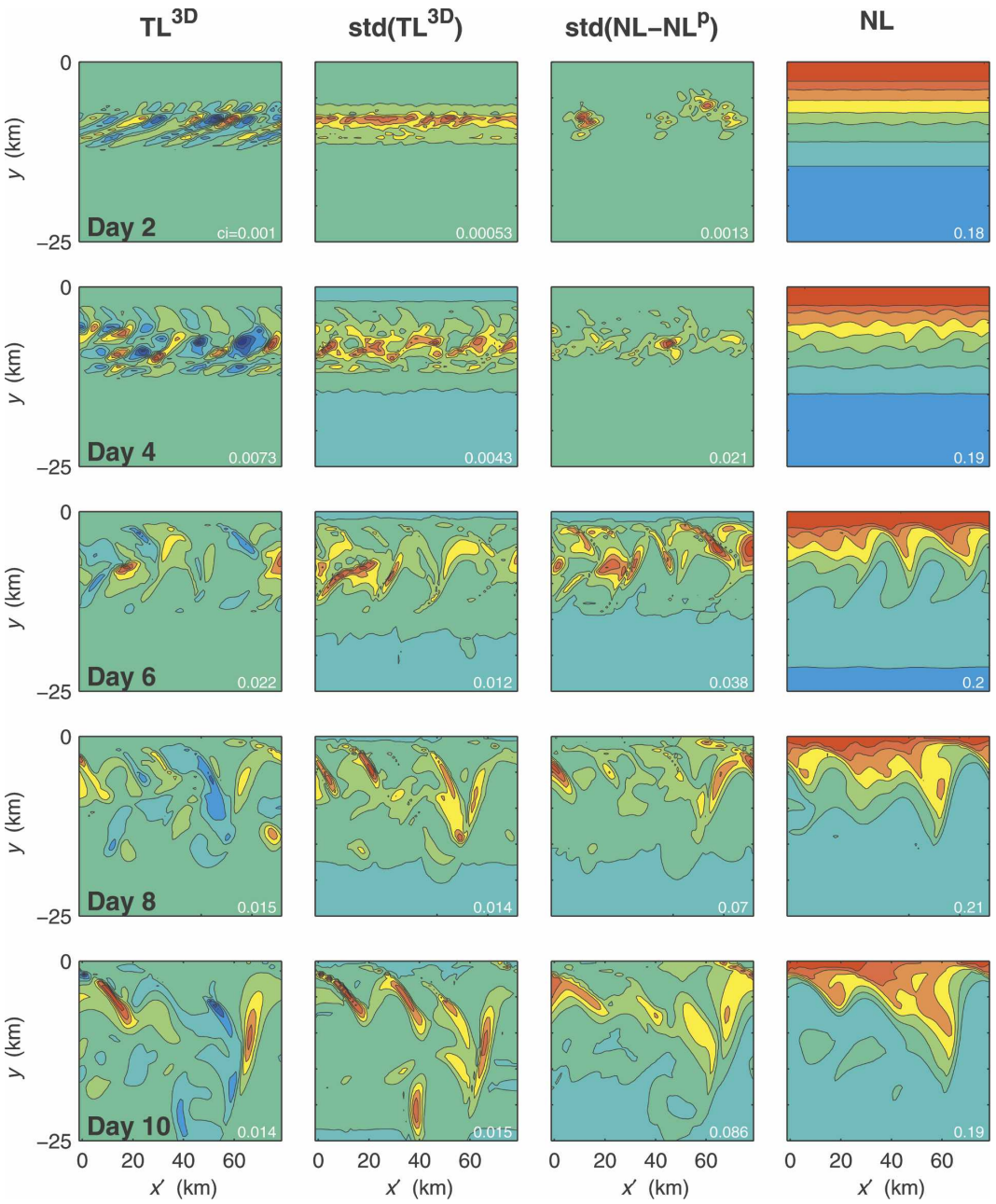

FIG. 8. (far left panels) Relaxed wind surface perturbation density signature of the disturbance evolution for a single realization of TL^{3D} along with (far right panels) surface density evolution for the corresponding perturbed nonlinear model; (second set of panels from left) standard deviation in the surface density fields in TL^{3D} over an ensemble of 15 simulations and (panels second from right) standard deviation in the surface density difference between the base nonlinear simulation and the ensemble of NL^{p} simulations. The 80-km region plotted tracks a propagating disturbance as it traverses the domain at a speed of approximately 0.28 m s^{-1}. Numbers in the lower-right corner of each panel indicate the contour interval for that frame; zero contour in the three left-hand sets of panels is indicated by the color offshore.

consistent with the nonlinear model evolution NL^{3D} (Fig. 8). The disturbance structures are similar (Figs. 7, 9) , the change in predominant scale is comparable, and the rates of change of energy have similar spectral character. This indicates that the observed scale change in the nonlinear model over the first 3 days is largely a result of adjustment of the mean flow to the changes in the wind forcing. At day 3 the prevalent tangent linear fields have slightly longer wavelength than the mean disturbance scale in the nonlinear model. Beyond this

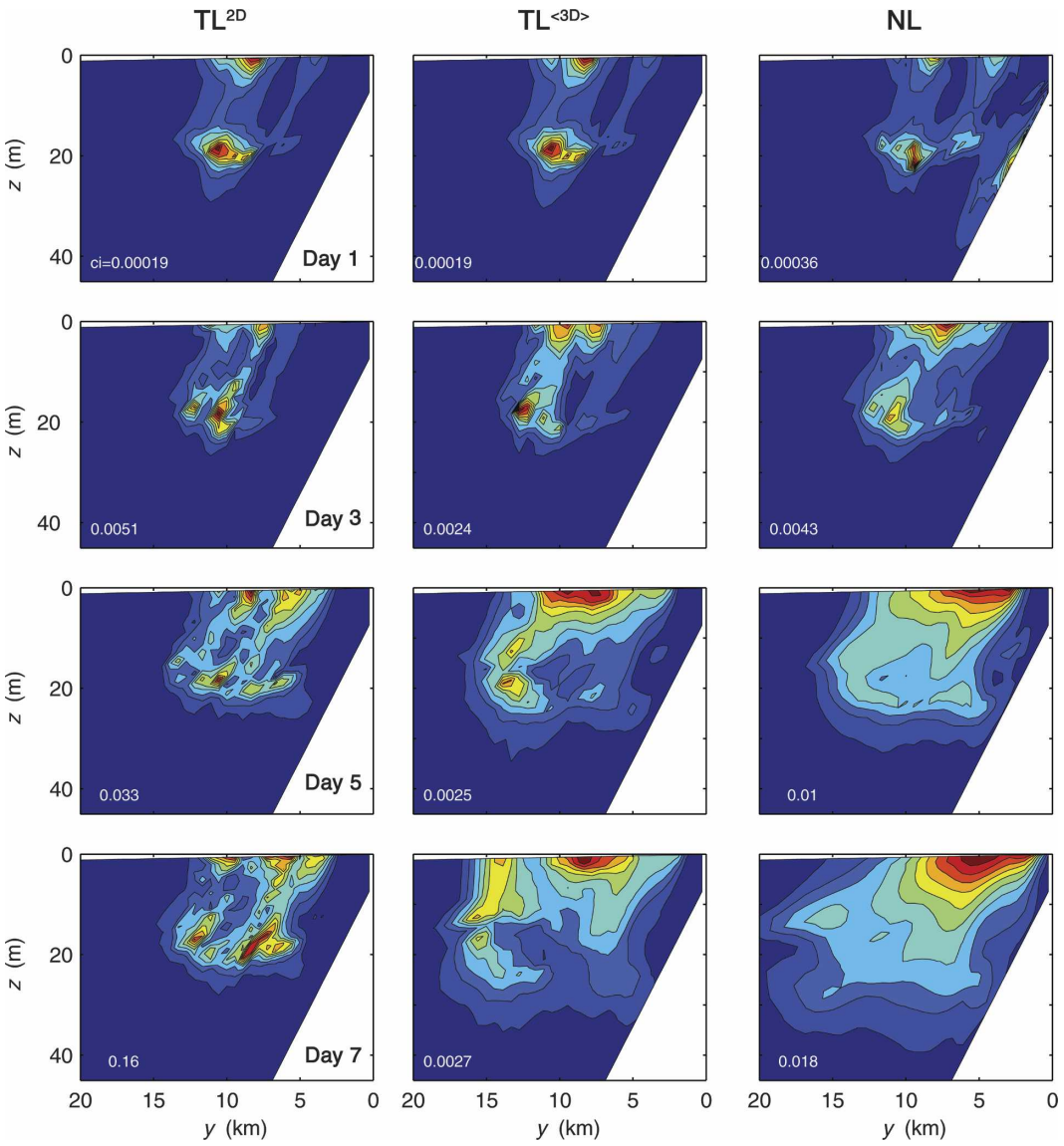

FIG. 9. Evolution under relaxed winds of the rms perturbation density for (left) the TL^{2D} simulation, (middle) a single realization of $TL^{\langle 3D\rangle}$, and (right) the base case NL simulation. Numbers in the lower-left corner of each panel indicate the contour interval for that frame (dark blue indicates near-zero values in all cases).

time, the TL^{2D} fields rebound moderately to higher k_{mean}, while in the nonlinear model the abrupt onset of growth at 20 km leads to a steady decline in k_{mean} (Fig. 6). The total perturbation energy $\tilde{E}_p$ in TL^{2D} exceeds the disturbance energy in the nonlinear model NL^{2D} by day 3 and continues to increase through day 10 (Fig. 5), indicating that a two-dimensionally relaxing upwelling front remains susceptible to linear disturbance growth for a significant period of time.

3) $TL^{\langle 3D\rangle}$ RESULTS

The $TL^{\langle 3D\rangle}$ simulations are similar to the TL^{2D} case in that the background flow is alongshore uniform and evolves in time due to the relaxation of the upwelling. However $TL^{\langle 3D\rangle}$ allows for the additional possibility that the finite-amplitude evolution of the disturbances may affect the instability characteristics by altering alongshore mean flow structure. As the amplitude of the frontal meanders increase, the alongshore-average steepness of the isopycnals in the front lessens and the mean intensity of the surface jet weakens (Fig. 3). Early in the relaxation process (day 2) the alongshore average background structure $S_o^{\langle 3D\rangle}$ strongly resembles the two-dimensional background state S_o^{2D} of TL^{2D} (Fig. 3). But as the frontal inflections grow in magnitude, $S_o^{\langle 3D\rangle}$ deviates from S_o^{2D}. The area-averaged (y–z) rms differ-

ence in density between the two solutions indicates that the rate at which $S_o^{\langle 3D\rangle}$ diverges from S_o^{2D} increases through approximately day 5, then remains roughly constant for the remainder of the simulation (Fig. 3).

Over the first 4 days of the simulation, the linear disturbance structures in $TL^{\langle 3D\rangle}$ bear strong similarity to those of TL^{2D} (Figs. 7, 9). The increasing divergence of the two background states leads to significantly different disturbance patterns by day 6. The $TL^{\langle 3D\rangle}$ disturbances change not only scale but shape, becoming more symmetric across the centerline of the alongshore jet. This evolution in surface density perturbation is similar to the patterns present in the deviation from the alongshore-average density of the nonlinear model (Fig. 7). After this point, the structures in the nonlinear model become increasingly irregular while the tangent linear disturbances broaden and weaken. The vertical and cross-shore pattern in the $TL^{\langle 3D\rangle}$ rms perturbation density retains a resemblance to the nonlinear solution longer than TL^{2D} does (Fig. 9). Though the magnitude of the perturbation density is less, at day 5, $TL^{\langle 3D\rangle}$ rms perturbation density shows similar surface intensification and depth structure as NL. By day 7, however, a region of intensification has developed 15 km offshore in $TL^{\langle 3D\rangle}$, which is not present in the nonlinear model.

Linear disturbance growth in $TL^{\langle 3D\rangle}$ exhibits the same tendency toward lower k_{mean} over the first 3 days as appeared for TL^{2D} (Fig. 5). But unlike in that case, k_{mean} decreases further between days 4.5 and day 8. The shift toward longer wavelengths past day 4 occurs concurrently with decay of energy at the prevailing scale (Fig. 6). This suggests that some of the subsequent NLM evolution in predominant wavenumber along the front between days 4.5 and 8 is associated with the finite-amplitude instabilities altering the structure of the alongshore mean background state. While nonlinear wave–wave interaction processes, which are not represented in $TL^{\langle 3D\rangle}$, undoubtedly play a significant role in determining the nature of the transitions between scales, it is clear that, at least through day 7 (when disturbance energy in $TL^{\langle 3D\rangle}$ ceases to increase), the alteration of the alongshore average background state promotes longer-wavelength instabilities. It is important to note, however, that disturbance growth is never supported in $TL^{\langle 3D\rangle}$ above approximately a 33-km wavelength. Thus, the transitions to the longest scales in NL^{3D} must necessarily involve transfer of energy from shorter scales.

4) TL^{3D} RESULTS

Unlike the TL^{2D} and $TL^{\langle 3D\rangle}$ cases, the background flow for TL^{3D} itself includes rapidly growing and evolving waves. Early in the disturbance evolution, TL^{3D} solutions (Fig. 8) resemble $TL^{\langle 3D\rangle}$ and TL^{2D} solutions (Fig. 7) because the wavelike structures in the background flow are initially very small relative to the alongshore mean circulation. However, as the frontal meanders in the basic flow amplify, disturbances in the TL^{3D} simulation transition into localized features about regions of sharp gradients in the background flow. An ensemble of 15 TL^{3D} simulations shows that there is significant variability among these patterns (Fig. 8). In any particular ensemble member, intense disturbance activity may develop about one amplifying meander of the front but not about another. Different ensemble members may show disturbance patterns that are quite similar in structure but opposite in sign. High linear disturbance variance tends to be associated with frontal inflections in the nonlinear solution, where meanders are extending rapidly offshore or are collapsing shoreward. Given that the TL^{3D} linear disturbances tend to indicate actively evolving regions in the developing background wave structures, it is not surprising that the mean scale of disturbance energy in TL^{3D} increases over time (Fig. 5). The rate of change of disturbance energy over the spectrum resembles the response of the nonlinear model more closely than TL^{2D} or $TL^{\langle 3D\rangle}$ (Fig. 6). This reflects disturbance growth at a preexisting scale in the background flow rather than amplification at a new scale.

A characteristic that the TL^{3D} and NLM simulations hold in common is the rate at which $\tilde{E}_p$ changes over the entire simulation (Fig. 5). After day 7, $\tilde{E}_p$ continues to increase in TL^{3D} and NLM while it is decreasing in $TL^{\langle 3D\rangle}$. The fact that it is decreasing in $TL^{\langle 3D\rangle}$ indicates that disturbances at a given wavenumber can no longer directly draw energy out of the alongshore mean flow. The continued rise of $\tilde{E}_p$ in the TL^{3D} simulations probably indicates the transfer of energy from the background waves to the linear perturbations. However, in the NLM simulations the increase in $\tilde{E}_p$ over the last several days of the simulation implies nonlinear transfer of energy from the mean flow.

5) NL^{p} RESULTS

Nonlinear perturbation experiments NL^{p} indicate that solutions of the full primitive equation model diverge rapidly from very similar initial states. These runs model the full nonlinear disturbance growth that TL^{3D} approximates linearly. For an ensemble of 15 simulations, the standard deviation in the difference fields bears similarity in structure to the standard deviation of disturbance field structures in the TL^{3D} experiments (Fig. 8) by day 4. The difference structures that develop from the NL^{p} relaxed wind experiments show clear cor-

relation with the strong gradients in the frontal features of the base case nonlinear simulation. In any particular ensemble member the difference fields develop irregularly along the front, emphasizing regions where the alongshore position of strong frontal meanders lag or lead those of the base case or where the offshore extent of an instability wave crest is extended or diminished. The consistency between TL^{3D} and NL^{p} solutions suggests that the linear approximation describes well the growth of perturbations in the fully nonlinear model. Thus, the predominant growing perturbations on the flow with finite-amplitude instabilities will tend to be phase and amplitude changes of the existing background structures. This is reminiscent of the findings of Snyder and Joly (1998), who noted that the fastest-growing perturbations (singular vectors in energy arid enstrophy norms) on a synoptic-scale baroclinic parent wave had final structures that represented shifts in phase and amplitude of the parent wave structure.

b. Sustained winds (case SW)

1) PERSISTENT WINDS

The unperturbed evolution of an upwelling front under persistent winds is characterized by offshore translation of the front and intensification of the coastal jet. As the front advects offshore, increasingly denser water upwells at the coast, and the near-vertical isopycnals in the frontal region extend deeper into the water column (Fig. 10). Over the 10-day simulation, the maximum velocity in the surface alongshore jet moves from approximately 6 to 13 km offshore.

The result of adding a small-amplitude perturbation to the initial state of the nonlinear model under sustained winds is the formation of frontal instabilities (Durski and Allen 2005). Over the first 3 days after the introduction of the disturbances, roughly 11-km-wavelength meanders amplify along the front (Fig. 11). As the frontal deflections become larger, the meanders interact, appearing to coalesce into larger scales. Qualitatively this is similar to the relaxed wind case. Over the first three days the predominant disturbance scale k_{mean} remains between 10 and 12 km (Fig. 12). Subsequently, a rapid progression to larger scale commences. This is in contrast to the wind relaxation experiments, which exhibited a nearly steady rate of change of wavenumber over the duration of the experiment. The enstrophy-weighted mean wavenumber k^{Z}_{mean} decreases comparably to k_{mean} after an initial rapid drop and recovery (Fig. 12).

Energy $\tilde{E}_p$ increases strongly in the disturbance scales over the first 3 days after introduction of the perturbation, followed by a gradually diminishing rate

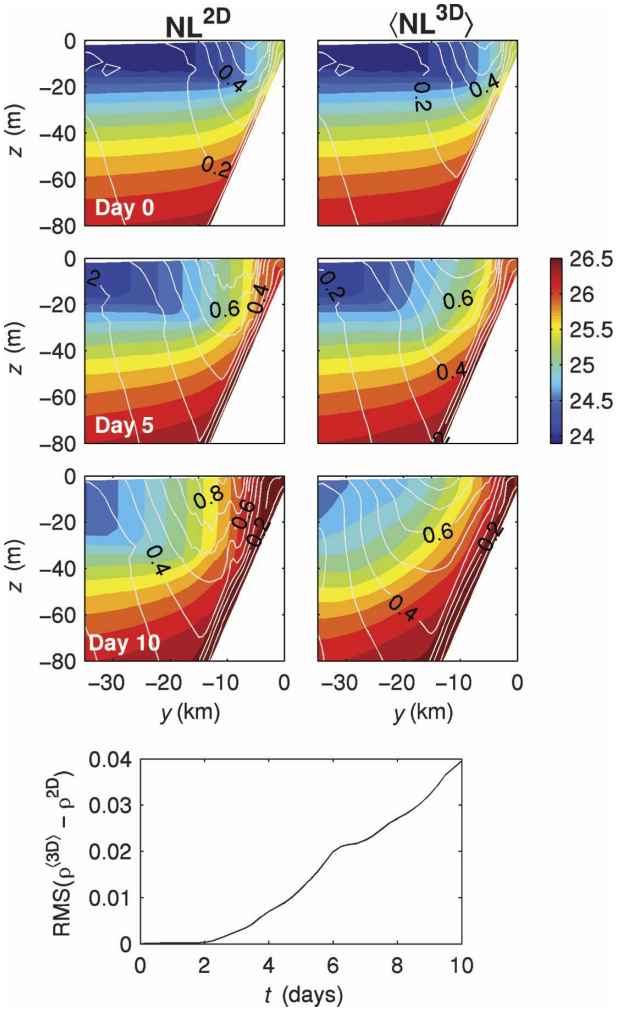

FIG. 10. (left-hand top three panels) Density (color contours) and alongshore velocity (line contours) structure in an across-shore section for days 0, 5, and 10 for the unperturbed nonlinear sustained wind experiment; (right-hand top three panels) alongshore averages of the same fields for a perturbed nonlinear sustained wind experiment. Fields represent the background states (left) S^{2D}_{o} and (right) $S^{\langle 3D\rangle}_{o}$. (bottom) The time series of the area (y–z) averaged rms difference in density between the two cases.

of increase over the remainder of the simulation (Fig. 12). The normalized rate of change of perturbation energy (Fig. 13) shows strong growth in the roughly 11–16-km waveband over the first four days, followed by a rapid transition to growth at greater than 30-km scale. Over the last 5 days of the simulation, the progression toward longer wavelength occurs through intermittent periods of growth and decay over portions of the lower part of the spectrum, suggesting that wave–wave interactions are transferring energy across the spectrum (Fig. 13).

The TL^{2D} steady wind run shows roughly 12-km scale structures preferentially forming on the onshore side of

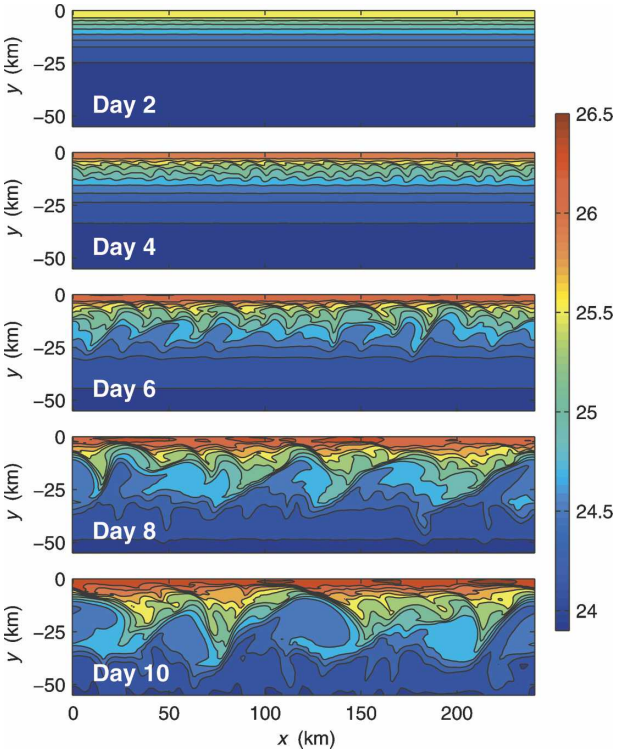

FIG. 11. Surface density contours depicting the evolution of the frontal instabilities in the nonlinear model sustained wind experiments.

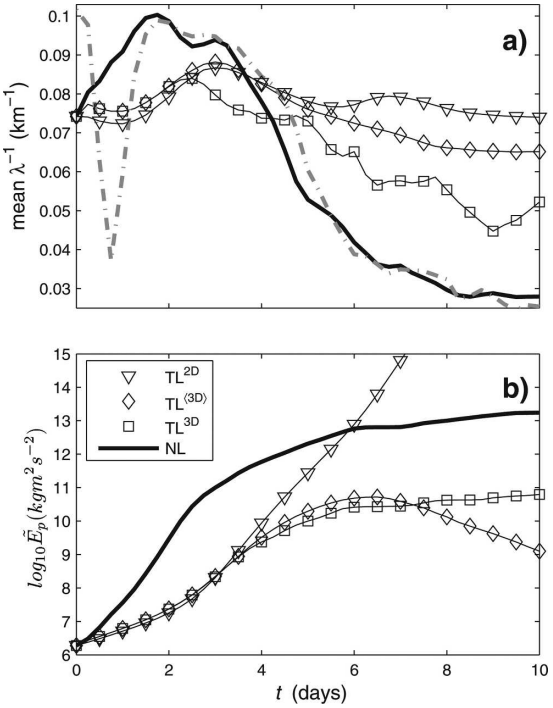

FIG. 12. (a) The mean alongshore wavenumber k_{mean} from Eq. (13) vs t for the sustained wind nonlinear and tangent linear experiments along with k^{Z}_{mean} from Eq. (14) (gray dash–dot line) for the NL experiment. (b) Total perturbation energy $\tilde{E}_p$ vs t for the sustained wind nonlinear and tangent linear experiments.

the surface jet maximum (Fig. 14), in contrast to the relaxed wind case in which disturbances preferentially developed with the opposite cross-shore slope offshore of the jet maximum (Fig. 7). The perturbations amplify rapidly at an approximately constant alongshore scale over the course of the simulation. The TL^{2D} simulation maintains a mean scale roughly between 11 and 13 km over the entire simulation (Fig. 12). None of the evolution to larger scale observed in the nonlinear model simulations is explained by the disturbance growth in this case. Interestingly, the characteristics of linear disturbance growth on the alongshore uniform upwelling front change less under sustained winds, for which the jet accelerates and advects offshore, than they do during relaxed winds for which the jet remains nearly stationary.

In the $TL^{\langle 3D\rangle}$ simulations the background state exhibits significant evolution as finite-amplitude instabilities grow to large magnitude (Fig. 10). The alongshore mean structure is characterized by increasingly flat isopycnals and diminishing horizontal and vertical shear in the frontal jet. The disturbance structures in $TL^{\langle 3D\rangle}$ gradually diverge from the TL^{2D} case, broadening and becoming more symmetric about the jet axis by day 6 (Fig. 14). But the features remain at relatively small scale throughout the simulation and bear little resemblance to the nonlinear model disturbance structures, even at day 4. In $TL^{\langle 3D\rangle}$, k_{mean} displays only a moderate and gradual decrease from 11- to 15-km wavelength over the last 7 days of the simulation (Fig. 12). These results are in contrast to the relaxed wind case in which much of the scale evolution of the nonlinear model could be explained in terms of the feedback between the finite-amplitude disturbances and the alongshore average basic-state flow. During the last 4 days, the total energy $\tilde{E}_p$ begins to decline. The scales that exhibited the fastest rate of increase of E_p over the first 6 days rapidly become damped (Fig. 13). This demonstrates that as the frontal instabilities grow, the alongshore average flow transitions from strongly unstable to stable. This is not surprising because, once the instabilities become of finite amplitude and the front exhibits significant meanders in the across-channel direction, the alongshore average flow does not retain the strong gradients in density and velocity that are associated locally with any position along the front.

Linear disturbance growth in the TL^{3D} simulations with a steady wind basic state show similar evolution as did those on a relaxing basic-state flow. The initial structures that develop (Fig. 15) resemble modes on an

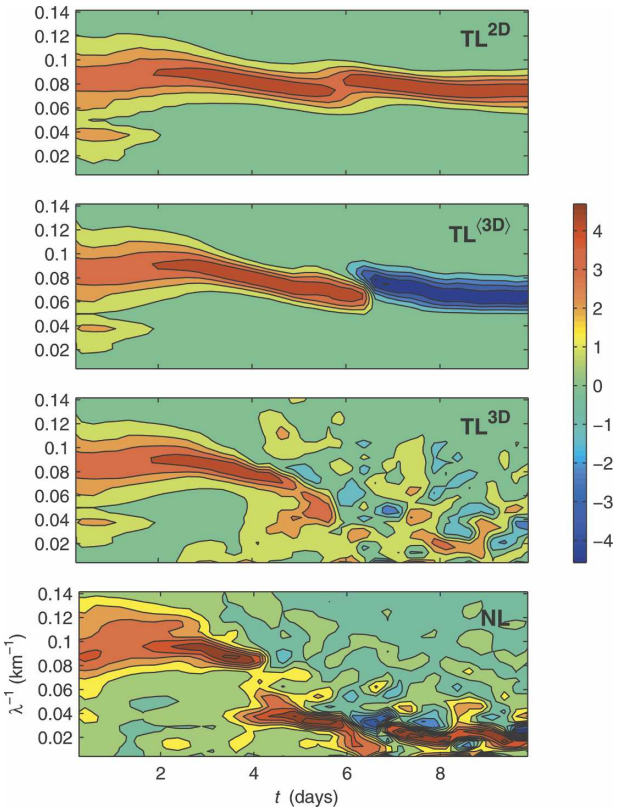

FIG. 13. The time rate of change of E_p as a function of wavenumber, normalized by the standard deviation of the rate of change at each time for the sustained wind nonlinear and tangent linear experiments.

alongshore uniform flow. Once finite-amplitude instabilities develop on the front in the basic state, the characteristics of the linear disturbances shift to correlate with the steep gradients of the wavelike background features. Once again, the standard deviation in the disturbance patterns bears resemblance to the standard deviation of differences between fields from the base-case nonlinear model and the slightly perturbed nonlinear model runs (Fig. 15) by day 4. The mean scale of disturbances gradually increases over the course of the simulation (Fig. 12), but does not reach the longest mean length scales of the nonlinear structures. Over the last 4 days of the simulation, the mean flow no longer supports significant instability growth, yet $\tilde{E}_p$ still gradually increases in both the nonlinear model and in the TL^{3D} simulations. This again indicates the importance of wave–wave–mean flow processes in promoting further amplification of frontal disturbances. The rate of change of disturbance energy $E_p(k)$ again shows that the linearized wave–wave interaction included in the TL^{3D} captures the tendency for energy to be transferred preferentially to longer wavelength (Fig. 13). But, the rapid scale transition that develops in the nonlinear model at day 4 is only partially captured in TL^{3D}. This suggests that the process on day 4 is highly nonlinear, involving very strong interaction between waves.

2) PARTIALLY SUSTAINED WINDS

Nonlinear model simulations were also performed in which the winds were relaxed to 0.0375, 0.025, and 0.0125 N m^{-2} (Fig. 1b). Interestingly, even with the wind relaxed to one-quarter of the original wind stress, the response in terms of scale change is much more similar to the persistent wind case than to the fully relaxed wind case. An initial increase in k_{mean}, followed by a rapid evolution to longer scale after approximately day 3, occurs similarly for partial wind relaxations of 0.0375, 0.025, and 0.0125 N m^{-2} (Fig. 16). This indicates a qualitative difference in the disturbance response, depending on whether the system is forced or unforced.

Despite the scale divergence of the fully relaxed solution from the others, the rate of increase of energy in the disturbances $\tilde{E}_p$ over the first 2 days is nearly identical in all cases (Fig. 16). Past day 2, disturbance energy increases more rapidly when the system is more strongly forced, suggesting that the winds are enhancing the disturbance amplification.

The TL^{3D} simulations were performed about the partial wind relaxation nonlinear background states. Again, the distinction between the disturbance response when some level of forcing is maintained, compared to when forcing is eliminated, is apparent in the evolution of mean disturbance length scale k_{mean} (Fig. 16). Over the first 3 days, total tangent linear disturbance energy $\tilde{E}_p$ increases most rapidly in the fully relaxed case and increases most slowly in the persistent forcing case. Evidently this variation in disturbance growth is related to the level of vertical mixing in the surface boundary layer where the instabilities develop. The presence of a well-mixed surface boundary layer in the experiments in which the wind forcing is partially or fully sustained leads to lower disturbance growth rate than in the zero-wind case. Indeed, repeating the steady wind tangent linear experiments with vertical mixing coefficients reduced by a factor of 100 results in linear disturbance growth rates over the first several days that are comparable to those of the relaxed wind tangent linear experiments. The rate of increase of disturbance energy in the NL sustained wind experiments over the first several days is also significantly higher than in the TL sustained wind experiments. This may indicate that wind forcing enhances disturbance growth through a nonlinear mechanism from very near the onset of the experiment or that the neglected term in the linearization of the vertical mixing is of significant magnitude.

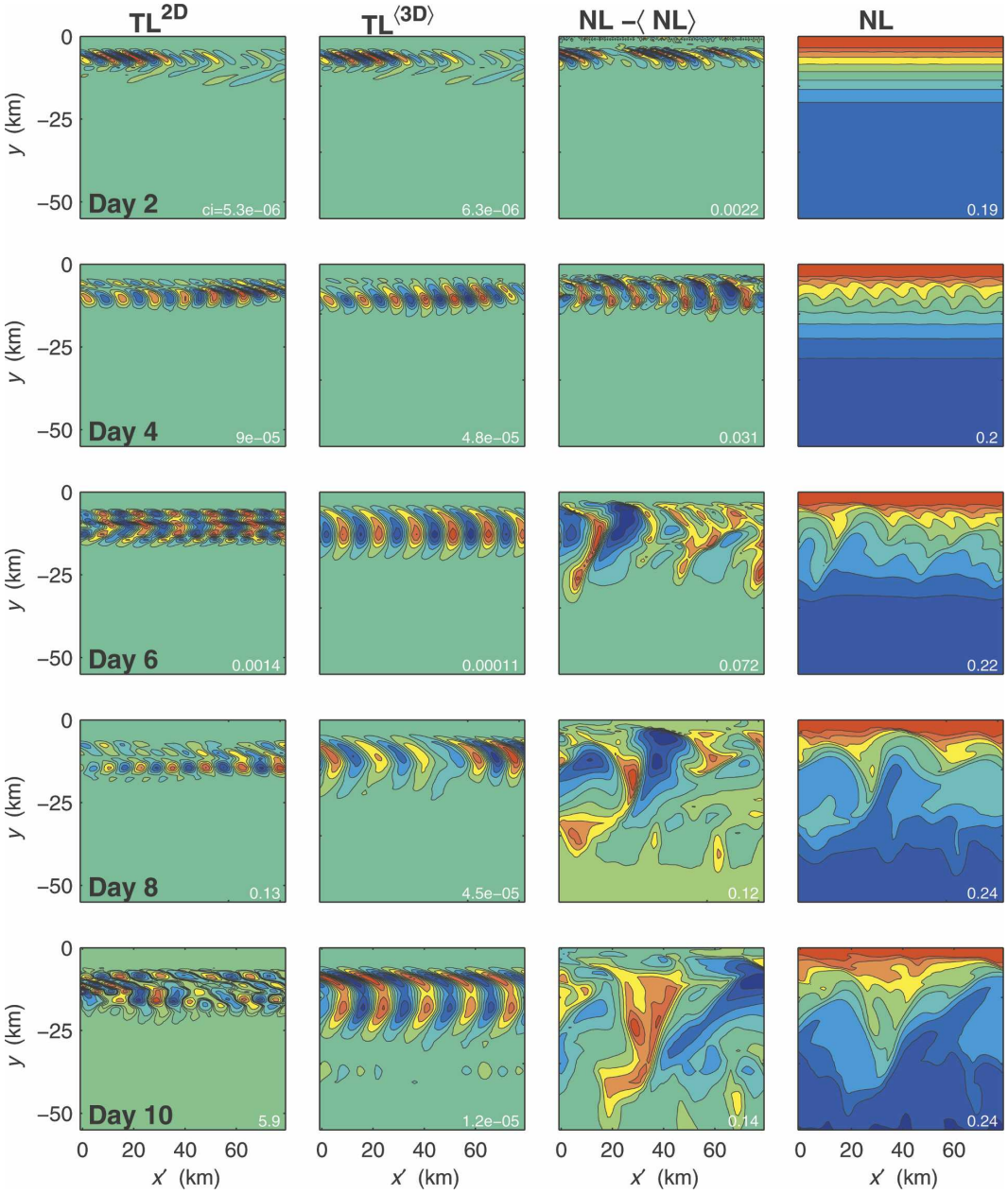

FIG. 14. Sustained wind, surface perturbation density signature of the disturbance evolution for the (far left panels) TL^{2D} simulation (panels second from right) and a single realization of $TL^{\langle 3D\rangle}$ along with (far right panels) surface density evolution for the corresponding perturbed nonlinear model and the (panels second from right) deviation from the alongshore average of the surface density in the nonlinear model. The 80-km region plotted tracks a propagating disturbance as it traverses the domain at a speed of approximately 0.66 m s^{-1}. The numbers in the lower-right corner of each panel indicate the contour interval for that frame; zero contour in the three left-hand sets of panels is indicated by the color offshore.

4. Summary

During the process of coastal upwelling, instabilities develop on upwelling fronts that introduce scales of variability in the alongshore direction. In numerical simulations of the phenomena in an alongshore uniform channel domain, disturbances first develop at approximately a 10-km scale but progress to 3–6 times that wavelength within 10 days (Durski and Allen 2005). This progression in scale occurs regardless of whether the wind stress is relaxed or maintained. The degree to which different aspects of the time-evolving

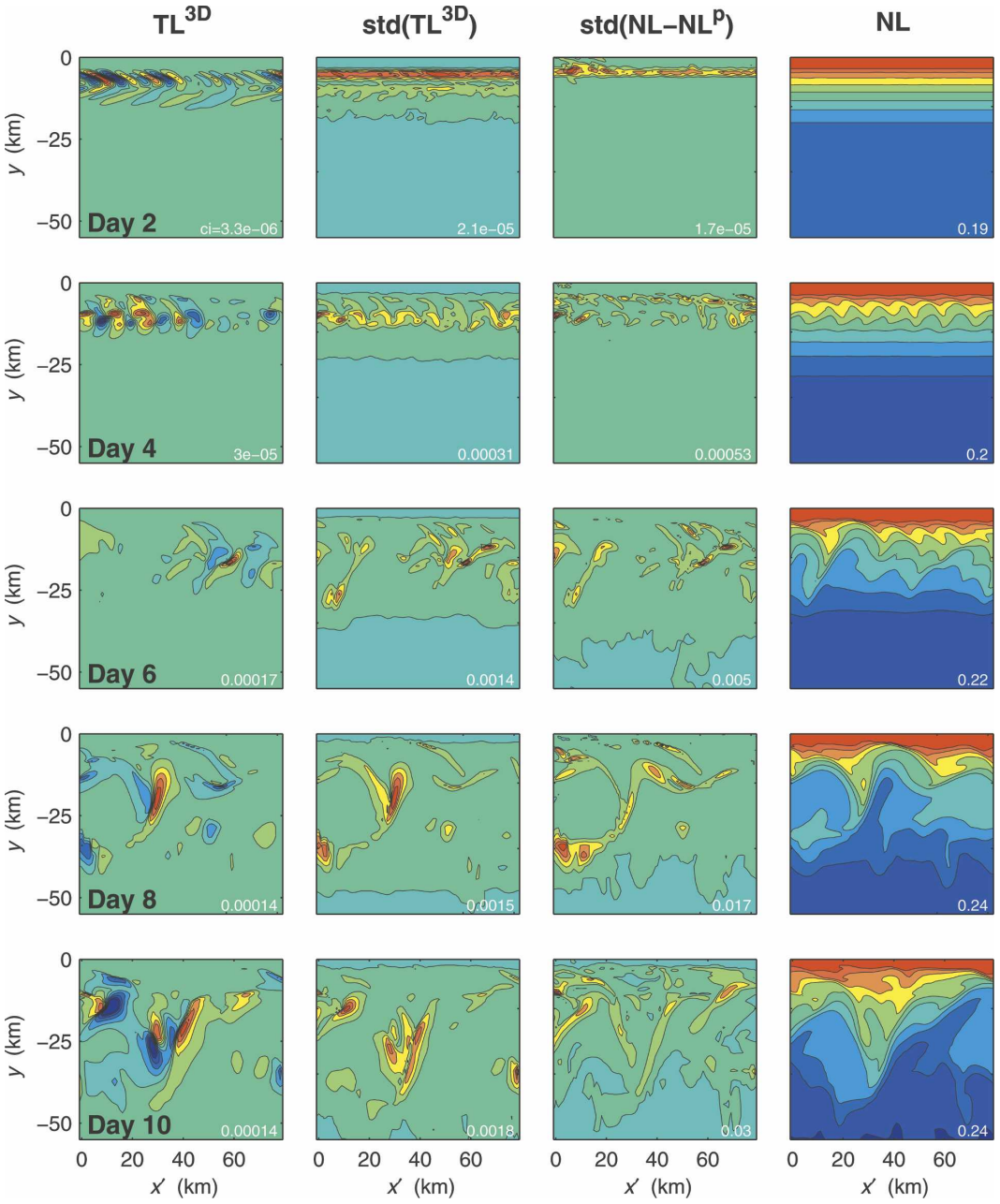

FIG. 15. Sustained wind surface perturbation density signature of the disturbance evolution for (far left panels) a single realization of TL^{3D} along with (far right panels) surface density evolution for the corresponding perturbed nonlinear model. (second set of panels from left) The standard deviation in the surface density fields in TL^{3D} over an ensemble of 15 simulations. (panels second from right) The standard deviation in the surface density difference between the base nonlinear simulation and the ensemble of NL^{p} simulations. The 80-km region plotted tracks a propagating disturbance as it traverses the domain at a speed of approximately 0.66 m s^{-1}. The numbers in the lower-right corner of each panel indicate the contour interval for that frame. The zero contour in the three left-hand sets of panels is indicated by the color offshore.

circulation account for this process is examined by comparison of the nonlinear solution characteristics to those of linear disturbances produced in tangent linear simulations. By utilizing different approximations to the full three-dimensional nonstationary nonlinear solution as the basic state for tangent linear simulations, the impact of different mechanisms in producing scale change is quantified.

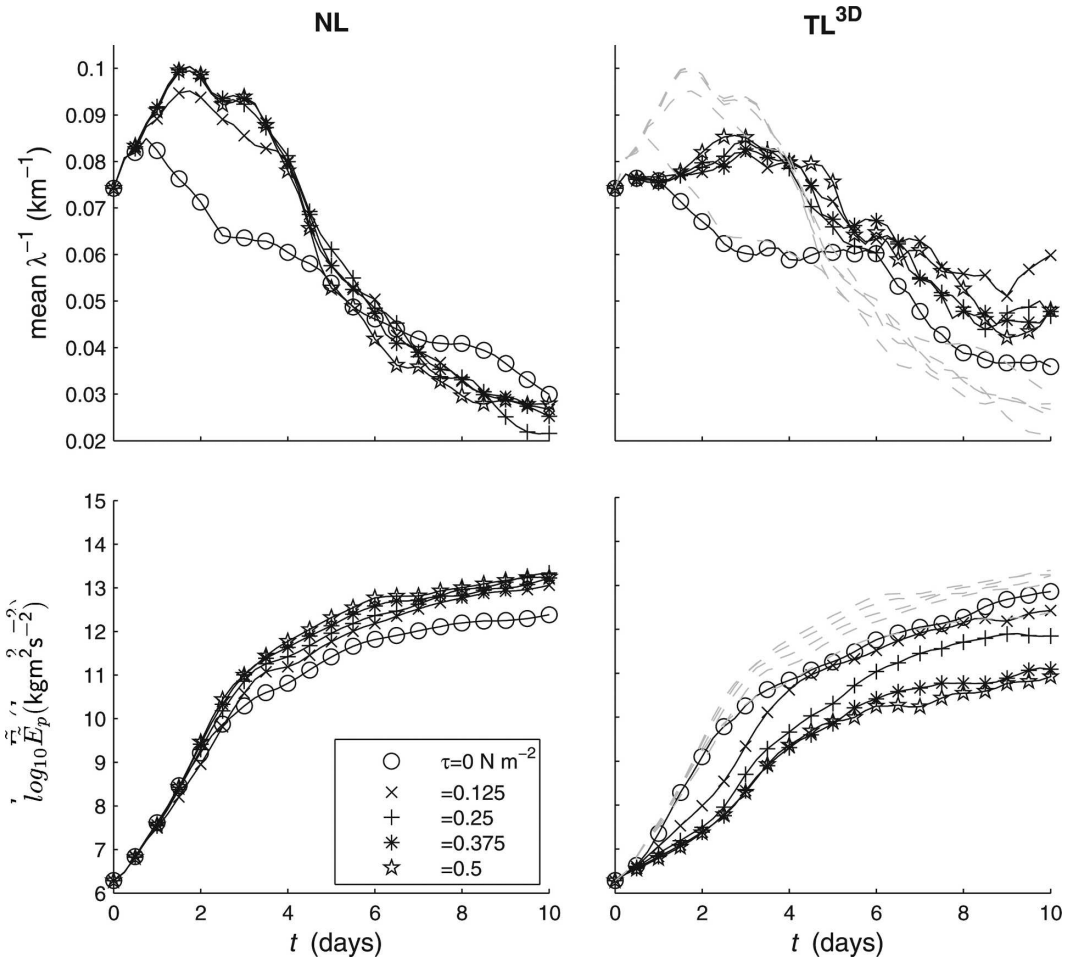

FIG. 16. (top) The mean alongshore wavenumber k_{mean} calculated using (13) for five different wind forcings for (left) the nonlinear model NL and (right) the TL^{3D} experiments; (bottom) total perturbation energy $\tilde{E}_p$ for these same experiments. Gray dashed lines in right-hand panels are the NL results from the left-hand panels, overlaid for ease of comparison.

The disturbance scale in the nonlinear simulations under relaxed winds increases more or less steadily over the duration of the 10-day simulation. The scale change over the first four days is very similar to that undergone by linear disturbances about a two-dimensional (unperturbed) relaxing front (S_o^{2D}). Between days 4 and 8, while linear disturbances about the (S_o^{2D}) state show no further scale change, the linear perturbation structures about the alongshore average of a three-dimensional basic state $S_o^{\langle 3D\rangle}$ continue to progress to larger scale. Thus, the feedback of the finite-amplitude growth of the disturbances alters the mean flow to favor disturbance growth at larger scale. These two processes, relaxation of the forcing and finite-amplitude wave–mean flow interaction, appear to explain a significant fraction of the scale change in the relaxed wind experiment up to about day 7. The subsequent adjustment must evidently be due to nonlinear wave–wave interaction effects.

The relative importance of different mechanisms for promoting scale change differs when the wind forcing is sustained. In this case, there is a rapid progression to larger scale, once the instabilities reach large amplitude. This occurs even when the upwelling favorable forcing is sustained at just a fraction of its initial strength. The scale change exhibited in the nonlinear model develops abruptly and progresses more rapidly to larger scale than in the relaxed wind case. The linear disturbances that evolve in the tangent linear experiments fail to track any significant portion of this scale change, indicating that the processes leading to scale evolution here are largely nonlinear.

The characteristics of the linear disturbances that develop on the full three-dimensional background state

(S_o^{3D}) under either relaxed or sustained winds resemble those of the alongshore-uniform approximations (S_o^{2D} and $S_o^{\langle 3D\rangle}$) for the first several days of the experiments. However as the frontal meanders in the basic state reach significant amplitude, the TL^{3D} perturbation structures evolve to reflect the presence of the increasing waviness of the background flow. Large linear disturbance magnitudes coincide with strong gradients in the meandering front. Disturbance growth reflects shift, amplification, or decay of a basic-state structure. This may indicate that an inherently nonlinear process, such as the merger of neighboring wave crests, is responsible for a portion of the scale change.

Acknowledgments. This research was supported by the National Science Foundation under Grant OCE-0218812. The authors are grateful to A. Moore and the ROMS tangent linear/adjoint code development team for helpful suggestions and their generosity in providing these programs.

REFERENCES

Barth, J. A., 1989a: Stability of a coastal upwelling front. 1. Model development and stability theorem. *J. Geophys. Res.,* **94,** 10 844–10 856.

——, 1989b: Stability of a coastal upwelling front. 2. Model results and comparison with observations. *J. Geophys. Res.,* **94,** 10 857–10 883.

——, 1994: Short-wavelength instabilities on coastal jets and fronts. *J. Geophys. Res.,* **99,** 16 095–16 115.

Durski, S. M., and J. S. Allen, 2005: Finite-amplitude evolution of instabilities associated with the coastal upwelling front. *J. Phys. Oceanogr.,* **35,** 1606–1628.

Eldevik, T., and K. B. Dysthe, 2002: Spiral eddies. *J. Phys. Oceanogr.,* **32,** 851–869.

Fukamachi, Y., J. P. McCreary, and J. A. Proehl, 1995: Instability of density fronts in layer and continuously stratified models. *J. Geophys. Res.,* **100,** 2559–2577.

Giering, R., and T. Kaminski, 1998: Recipes for adjoint code construction. *ACM Trans. Math. Software,* **24,** 437–474.

McCreary, J. P., Y. Fukamachi, and P. K. Kundu, 1991: A numerical investigation of jets and eddies near an eastern ocean boundary. *J. Geophys. Res.,* **96,** 2515–2534.

Mellor, G. L., and T. Yamada, 1982: Development of a turbulence closure model for geophysical fluid problems. *Rev. Geophys.,* **20,** 851–875.

Moore, A. M., H. G. Arango, E. D. Lorenzo, B. D. Cornuelle, A. J. Miller, and D. J. Neilson, 2004: A comprehensive ocean prediction and analysis system based on the tangent linear and the adjoint of a regional ocean model. *Ocean Modell.,* **7,** 227–258.

Shchepetkin, A. F., and J. C. McWilliams, 2003: The regional ocean modeling system: A split-explicit, free-surface, topography-following coordinate ocean model. *J. Geophys. Res.,* **108,** 3090, doi:10.1029/2001JC001047.

Shepherd, T. G., 1993: A unified theory of available potential energy. *Atmos.–Ocean,* **31,** 1–26.

Shi, X. B., and L. P. Roed, 1999: Frontal instabilities in a two-layer, primitive equation ocean model. *J. Phys. Oceanogr.,* **29,** 948–968.

Snyder, C., and A. Joly, 1998: Development of perturbations within growing baroclinic waves. *Quart. J. Roy. Meteor. Soc.,* **124,** 1961–1983.